Supplementary Information: "A tempered fractional Hawkes framework for finite-memory drought dynamics"

November 3, 2025

Mauricio Herrera-Marín^{1†}

¹Faculty of Engineering, Universidad del Desarrollo, Santiago, Chile [†]Correspondence: mherrera@udd.cl

S1. Parameter co-variability: μ , κ , and α

Figure S1 shows the empirical correlation matrix between the baseline rate μ , the excitation amplitude κ , and the fractional order α , computed across all analyzed grid points.

Two features are particularly noteworthy. First, α and κ are strongly anti-correlated $(r \approx -0.82)$, indicating that regions with strong self-excitation (large κ) tend to exhibit low fractional order α and therefore slow memory decay. In other words, locations where each dry-spell onset substantially reinforces the probability of subsequent onsets are also locations where that influence persists for a long time. This joint signature supports the interpretation of these regions as dynamically fragile: once dryness emerges, it is both self-sustaining (large κ) and slow to relax (small α).

Second, μ shows only weak-to-moderate correlation with α and κ ($|r| \lesssim 0.25$). This implies that the exogenous hazard of dry-spell initiation (how often onsets occur spontaneously) is, to first order, statistically decoupled from the persistence structure and reinforcement strength. In physical terms, climatological aridity (large μ) does not by itself guarantee long memory; memory is instead an emergent dynamical property, governed by coupling, feedback, and synoptic organization.

S2. Station-scale dynamics: intensity, kernel, and parameter triplets

To illustrate the physical meaning of the inferred parameters, Figure S2 shows, for each medoid station, three elements: (i) the mean conditional intensity m(t) predicted by the fractional Hawkes model under a representative external forcing pulse sequence, (ii) the corresponding memory kernel $\phi(h) \propto h^{-\alpha}$ (and its exponentially tempered version $\phi(h) \propto h^{-\alpha}e^{-\theta h}$ for interpretability), and (iii) the parameter triplet (μ, κ, α) for that station.

These panels highlight how stations in climatologically stressed regions simultaneously (a) exhibit elevated κ (event-to-event reinforcement), (b) display small α (slow decay of

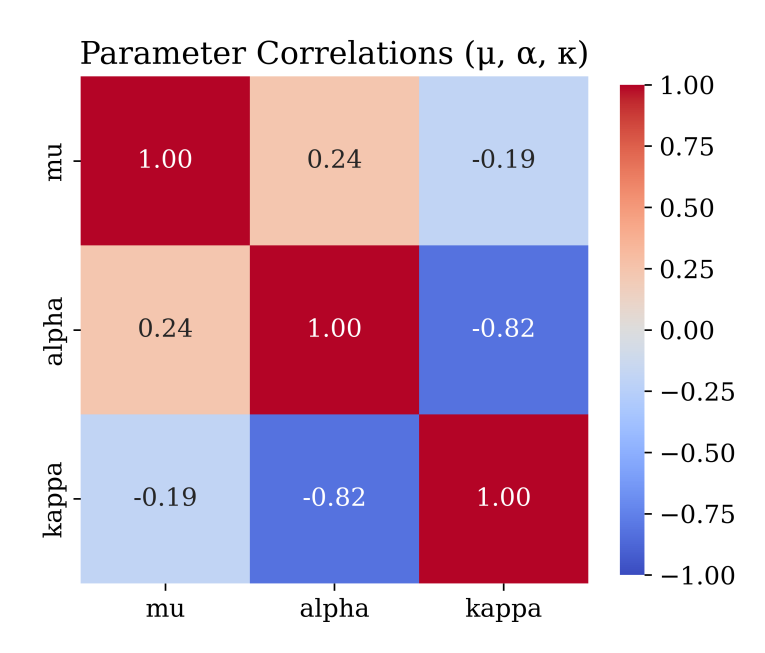


Figure S1. Correlation matrix between μ (baseline rate), α (fractional memory order), and κ (excitation amplitude). The strong negative correlation between α and κ indicates that regions of strong self-excitation also exhibit slow memory decay (small α), i.e. persistent drought dynamics.

memory), and (c) maintain intensities that do not immediately relax back to the baseline μ after an external burst. In contrast, stations with larger α show a much more rapid post-burst decay toward μ , approximating a short-memory or quasi-Markovian response.

S3. Temporal response and the role of tempering

To illustrate the dynamical implications of fractional versus tempered memory, Fig. S3 compares the mean intensity m(t) (left panels) and the corresponding memory kernels $\phi(h)$ (right).

The pure fractional kernel (orange line) decays as a power law $\phi(h) \propto h^{-\alpha}$, allowing the influence of past events to persist indefinitely and leading to slow, cumulative growth of intensity under sustained excitation. Introducing exponential tempering $e^{-\theta h}$ (blue line) truncates the long tail, producing a finite-memory system that saturates after a characteristic timescale $\tau_m = 1/\theta$. This tempering regularizes the fractional process, enforcing dynamic stability ($\eta < 1$) while preserving scale-free clustering over intermediate timescales. Physically, the tempering mimics processes such as seasonal hydrological resetting or circulation regime shifts that limit effective climatic memory.

S4. Parameter dependence on elevation

Elevation modulates several hydroclimatic controls, including orographic uplift, storm-track exposure, snow-rain partitioning, and soil moisture availability. Figure S5 plots μ , κ , and α as functions of station elevation (altitude above mean sea level). Each panel includes individual stations and a smooth low-order polynomial fit.

Two robust tendencies emerge. First, μ generally decreases with elevation, consistent

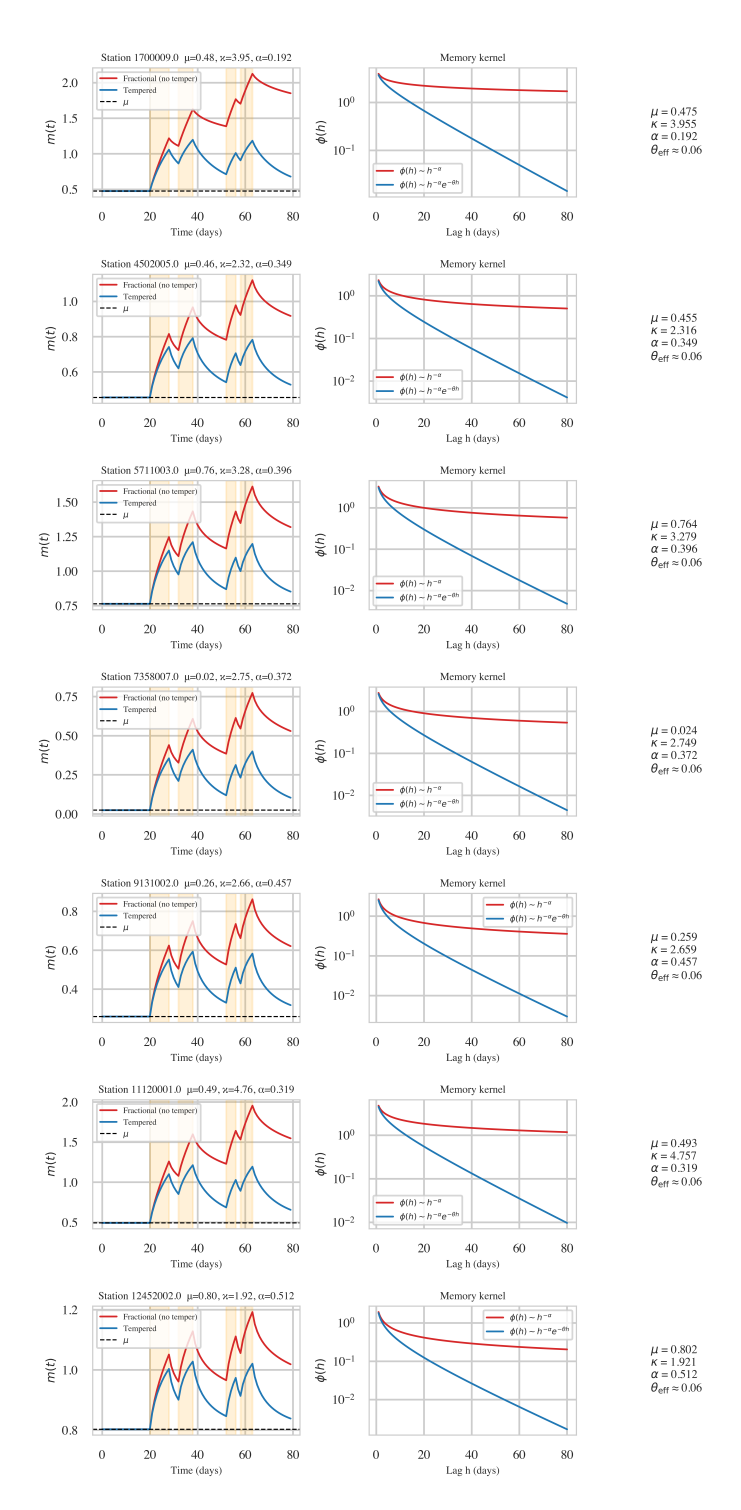


Figure S2. For each medoid station: (left) modeled mean intensity $\lambda(t)$ following a sequence of exogenous forcing bursts (shaded intervals); (middle) memory kernels for the same station, comparing pure fractional $(h^{-\alpha})$ and tempered fractional $(h^{-\alpha}e^{-\theta h})$ responses; (right) the fitted parameters (μ, κ, α) with station ID. Stations with small α and large κ exhibit slow decay and strong endogenous reinforcement.

with the fact that high-elevation sites in southern/Andean sectors experience frequent precipitation events (i.e. fewer "dry onset" days). Second, α tends to increase with elevation, implying faster memory decay at high topographic sites. In other words,

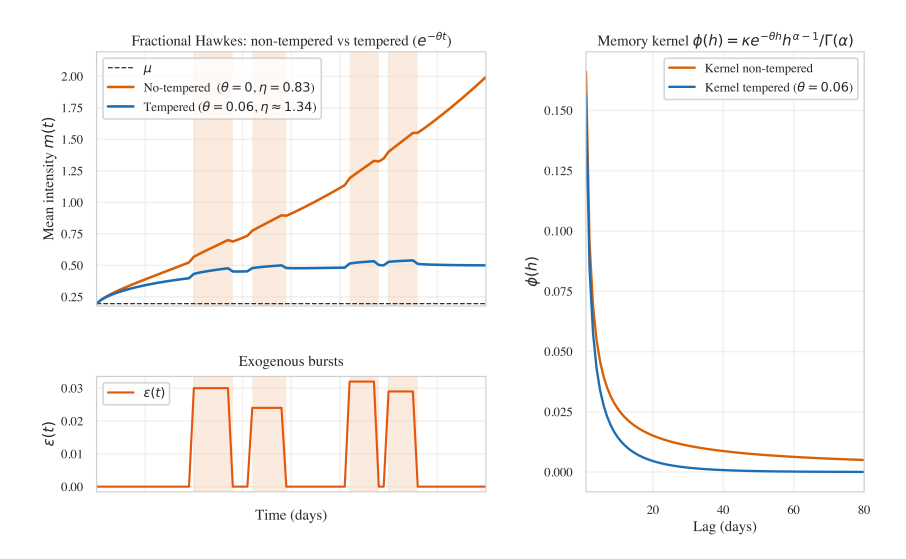


Figure S3. Comparison between non-tempered and tempered fractional Hawkes dynamics. Left: mean intensity $\lambda(t)$ under successive external pulses (shaded bands), showing unbounded accumulation in the pure fractional case (orange) and stable saturation in the tempered case (blue). Right: corresponding memory kernels $\phi(h)$, illustrating the transition from power-law persistence $(h^{-\alpha})$ to exponentially tempered memory with finite horizon $\tau_m = 1/\theta$.

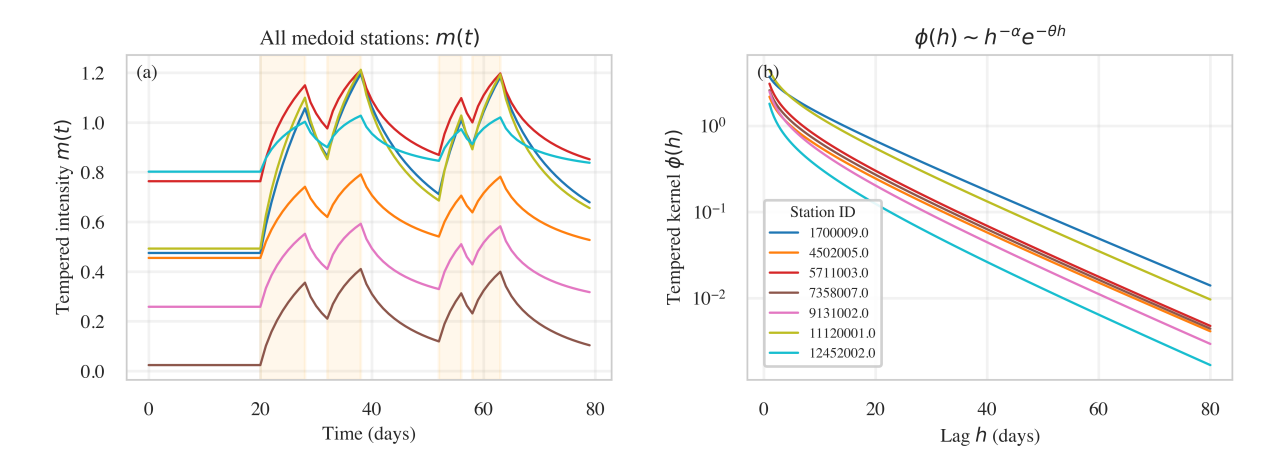


Figure S4. Comparative memory structure across medoid stations. (Left) Mean conditional intensity m(t) for all medoid stations subjected to the same sequence of synthetic exogenous bursts, illustrating how rapidly (or slowly) each station relaxes back toward its baseline rate μ . (Right) Corresponding memory kernels $\phi(h)$ on a logarithmic scale, including both non-tempered (power-law $h^{-\alpha}$) and exponentially tempered ($h^{-\alpha}e^{-\theta h}$) forms. Stations with shallower kernel slopes (smaller α) retain the influence of past drought onsets far longer than those with steeper kernels (larger α). Medoid stations are representative locations selected from distinct hydroclimatic regions to capture the diversity of dynamical regimes observed across the Chilean domain. This comparative overlay highlights that drought memory depth and self-excitation strength are station-specific, spatially structured, and quantifiable within the tempered fractional Hawkes framework.

mountainous locations behave more "forgetfully": dry spells there relax more quickly,

plausibly reflecting efficient replenishment by frontal systems and reduced persistence of blocking at those latitudes and altitudes. The amplitude κ shows localized maxima at intermediate elevations, suggesting that self-excitation is strongest where land–atmosphere coupling and synoptic-scale forcing coexist (e.g. transitional Andean foothills), but not necessarily at the highest peaks nor at the coastal plain.

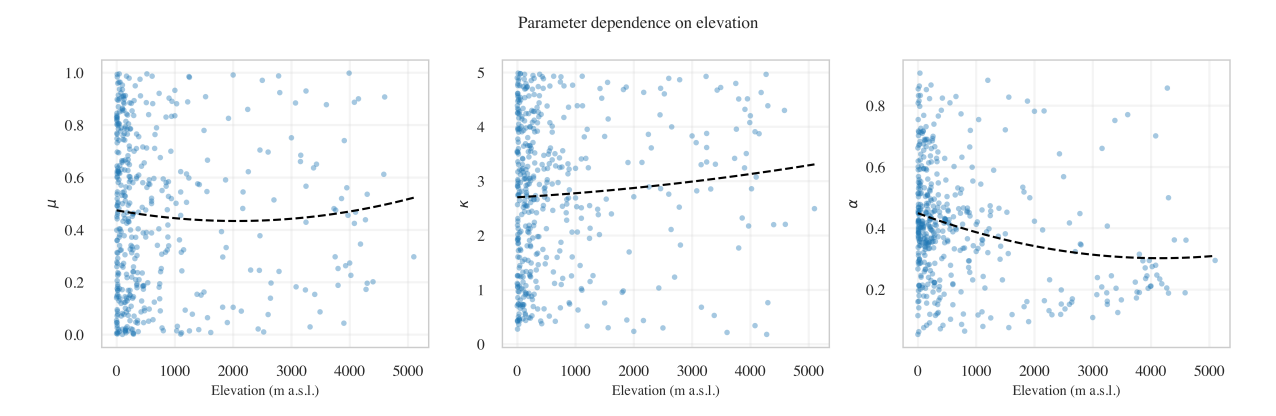


Figure S5. Baseline rate μ , excitation amplitude κ , and fractional order α as a function of station elevation. Points denote individual stations; curves show smoothed polynomial fits. High-elevation regions tend to have lower μ (fewer dry-start days) and larger α (shorter memory), consistent with rapid hydrometeorological reset.

S5. Parameter dependence on coastal proximity

Moisture delivery in Chile is strongly controlled by westerly flow, marine boundary-layer structure, and coastal upwelling. To assess how proximity to the Pacific coast modulates drought onset dynamics, we estimate the coastal distance for each grid point and examine μ , κ , and α as functions of that distance (Fig. S6).

Near the coast, μ is typically lower in the south (frequent precipitation, few dry onsets) but can remain elevated in the arid north where coastal subsidence and cold upwelling inhibit convection. Farther inland, κ tends to increase in the transitional belts, indicating that once dryness is established inland, it is more likely to self-reinforce. Meanwhile, α often decreases inland in the subtropics, implying slower memory decay (i.e. longer persistence of dryness away from immediate marine influence). These gradients underscore that the memory structure of drought is not purely zonal/latitudinal, but also reflects distance from the coastal moisture source.

S6. Regionalized distributions of fitted parameters

Finally, Figure S7 summarizes the distributions of μ , κ , and α across broad meridional sectors ("North", "Central", "South"), defined by latitude bands. For each sector we show violin or box plots of each parameter.

This view emphasizes that: (i) the arid north is characterized by high μ (high external dry-onset frequency), high κ (strong endogenous reinforcement), and low α (slow memory decay), i.e. long-lived and self-sustaining dry regimes; (ii) the central sector is heterogeneous, reflecting the coexistence of Mediterranean dryness and episodic frontal

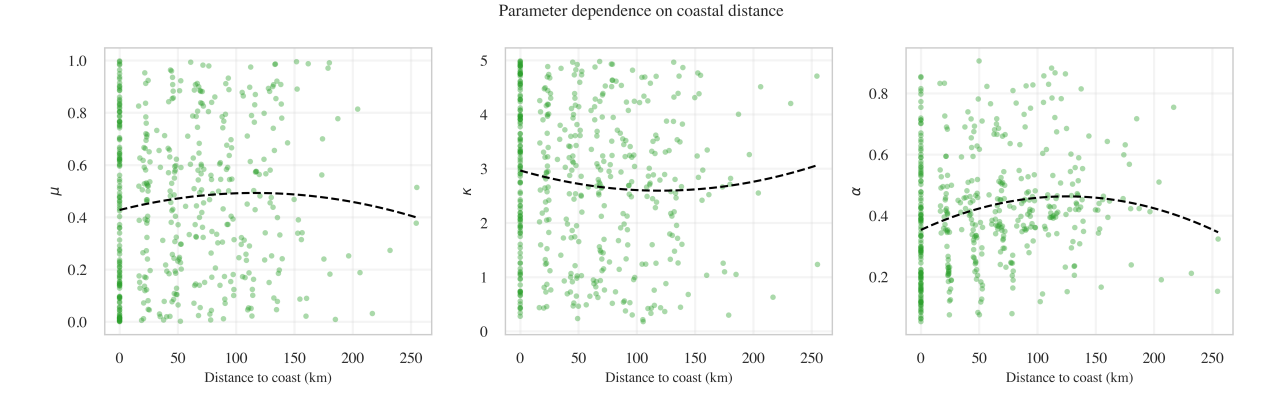


Figure S6. Dependence of μ , κ , and α on estimated coastal distance. Points represent stations; lines denote smoothed fits. Inland regions in the subtropical belt tend to show stronger self-excitation (κ) and slower memory decay (smaller α).

influence; and (iii) the south exhibits lower κ and higher α , consistent with externally forced, fast-reset droughts. These contrasts justify the interpretation of the fractional Hawkes parameters as physically meaningful climate diagnostics, not merely statistical fit parameters.

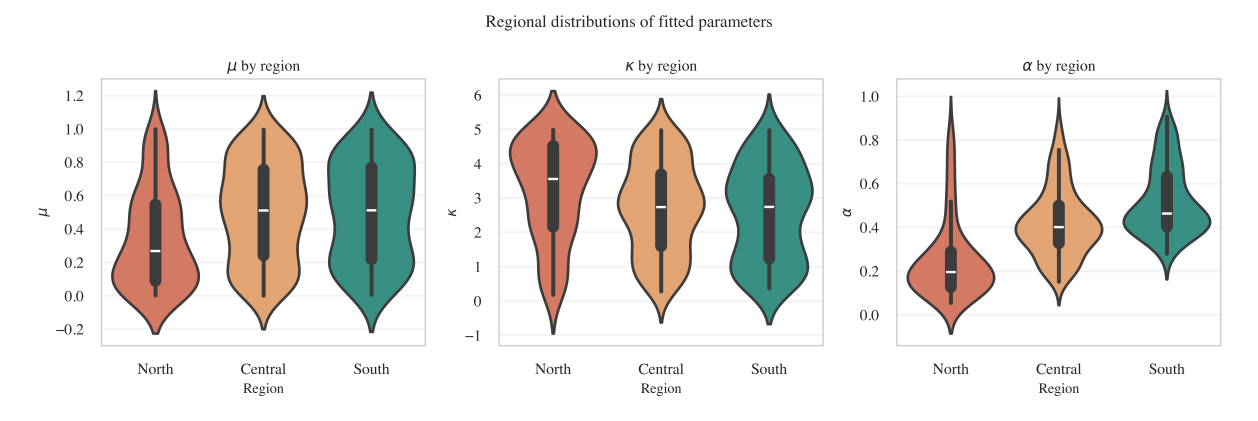


Figure S7. Regional distributions (e.g. North, Central, South) of μ , κ , and α , shown as violin/box plots. The north clusters in the regime "high μ , high κ , low α ," indicating persistent, self-reinforcing dryness. The south clusters near "low μ , low κ , high α ," indicating externally forced, fast-decaying dry spells.

Taken together, these supplementary diagnostics corroborate the main text: drought onset dynamics in this framework cannot be reduced to a single scalar metric such as "aridity." Instead, persistence (via α), reinforcement (via κ), and baseline hazard (via μ) co-vary in physically interpretable ways across geography, elevation, and coastal influence.